The effect of wall slip on the dynamics of a spherical particle in Newtonian and viscoelastic fluids subjected to shear and Poiseuille flow

The effect of wall slip on the dynamics of a spherical particle in Newtonian and viscoelastic fluids subjected to shear and Poiseuille flows

Marco Trofa*

Dipartimento di Ingegneria Chimica, dei Materiali e della Produzione Industriale, Università di Napoli Federico II, P.le Tecchio 80, 80125 Napoli, Italy

Center for Advanced Biomaterials for Healthcare @CRIB, Istituto Italiano di Tecnologia, Largo Barsanti e Matteucci 53, 80125 Napoli, Italy

Gaetano D'Avino

Dipartimento di Ingegneria Chimica, dei Materiali e della Produzione Industriale, Università di Napoli Federico II, P.le Tecchio 80, 80125 Napoli, Italy

Martien A. Hulsen

Department of Mechanical Engineering, Eindhoven University of Technology, PO Box 513, 5600 MB Eindhoven, The Netherlands

Pier Luca Maffettone

Dipartimento di Ingegneria Chimica, dei Materiali e della Produzione Industriale, Università di Napoli Federico II, P.le Tecchio 80, 80125 Napoli, Italy

Abstract

We address the effect of wall slip on the dynamics of a spherical particle suspended in an inertialess Newtonian or viscoelastic shear-thinning fluid under shear or Poiseuille flow. The study is performed through 3D direct finite element simulations by employing an Arbitrary Lagrangian-Eulerian

*Corresponding author. Tel.: +39 0817682280

Email addresses: marco.trofa@unina.it (Marco Trofa), gadavino@unina.it (Gaetano D'Avino), m.a.hulsen@tue.nl (Martien A. Hulsen), pierluca.maffettone@unina.it (Pier Luca Maffettone)

method for the particle motion.

In both shear and Poiseuille flows, wall slip reduces the difference between the particle translational velocity along the flow direction and the velocity of the unperturbed fluid, and slows down the particle rotational velocity. Remarkably, in a viscoelastic fluid, the presence of wall slip reverses the migration direction as compared to the no-slip case. Hence, for sufficiently high slip coefficients, all the particles migrate toward the channel midplane in shear flow and toward the channel centerline in Poiseuille flow, regardless of their initial position through the channel.
Keywords: Slip boundary condition, Particle migration, Viscoelasticity, Shear flow, Poiseuille flow, Numerical simulations

---

1. Introduction

In the last decades, a growing interest in microfluidics, i.e., a technology characterized by the engineered manipulation of fluids at the sub-millimeter scale, has been observed [1, 2]. This technology, indeed, has a number of advantages as compared to macroscopic systems such as a fine tuning of flow and transport conditions and the capability to handle micrometric particles, which are fundamental in both synthesis and analysis.

An important aspect when dealing with suspensions flowing in microfluidic devices is the precise manipulation of particle trajectories. In this regard, a primary operation in several microfluidic applications is the so-called 3D particle focusing, i.e., the controlled alignment of particles along one streamline of the flow field. As such, particle focusing has been widely studied and many methods to promote particle alignment have been proposed [3].

A promising technique to induce particle alignment is based on the use of viscoelastic fluids as suspending medium in microfluidic devices [4]. Indeed, 3D focusing [5, 6, 7] has been proven to be easily feasible in straight microchannels by suspending particles in viscoelastic liquids. Fluid elasticity, in fact, induces a cross-streamline particle migration, i.e., a motion of the suspended particles transversally to the main flow direction, that can be efficiently exploited to concentrate particles in some specific region of the channel cross-section. The migration direction depends on several parameters such as the flow field, the flow intensity, and the fluid rheological properties [4]. In general, in tube flow, the suspended particles move toward the wall or the centerline depending on their initial position, and fluid shear-thinning promotes particles at wall [6, 4]; in shear flow, they migrate toward the nearest wall [8].

In most of the theoretical and numerical studies on the dynamics of single, rigid particles in viscoelastic liquids, the validity of the no-slip boundary condition at all solid-fluid interfaces is assumed. However, at small scales [9, 10] and with complex fluids [11, 12], boundary slip, i.e., a discrepancy between the fluid velocity and the velocity of the solid surface immediately in contact with it, may occur. Slip at a solid-fluid interface modifies both the fluid velocity profile and the fluid-particle hydrodynamic interactions, affecting, in turn, the particle migration phenomenon [11].

The simplest slip boundary condition has been proposed by Navier [13] and defines a linear relationship between the tangential components of the fluid velocity at the boundary and the traction acting tangentially to the surface, the proportionality being ruled by a 'slip coefficient'. The Navier boundary condition has been used to study the effect of the slip on the

creeping motion of a spherical particle suspended in a Newtonian fluid near a flat wall [14, 15] or in a circular cylindrical pore [16]. In general, both slip on the particle surface and on the wall reduce the drag on the particle.

Our group has recently investigated the effect of the slip at the particle-fluid interface on the dynamics of a rigid sphere in an inertialess viscoelastic fluid under shear and Poiseuille flow [17]. No-slip condition was imposed at the channel walls. In both flows, particle slip reduces the difference between the particle translational velocity along the flow direction and the velocity of the unperturbed fluid at the same position, and speeds up the particle rotation with respect to the no-slip case. Furthermore, in shear flow, particle slip only affects the migration velocity magnitude, which, for increasing values of the slip coefficient, reaches a maximum and then decreases to values lower than the no-slip one. In Poiseuille flow, the migration dynamics qualitatively changes as compared to the no-slip case for sufficiently high slip coefficients: the tube wall becomes an unstable equilibrium position, and the particle migrates toward the channel centerline for any initial position through the channel.

The present paper reports results complementary to our previous one [17], i.e., here we consider no-slip condition at the particle-fluid interface and a slip condition at the channel walls. Specifically, we present 3D numerical simulations on the dynamics of a neutrally-buoyant spherical particle suspended in an inertialess viscoelastic fluid, both under shear and Poiseuille flows, with slip on the channel walls, with specific interest on the particle migration phenomenon. The governing equations are solved through the finite element method, with an Arbitrary Lagrangian-Eulerian (ALE) approach to

handle the particle motion. The particle translational and angular velocities as a function of the particle position through the channel are presented in terms of mastercurves for different wall-fluid slip coefficients.

2. Governing equations

The two problems studied in this work are schematically presented in Fig. 1: a single, rigid, non-Brownian, spherical particle moves between two parallel plates in shear flow (Fig. 1a) or in a cylindrical tube in Poiseuille flow (Fig. 1b). A Cartesian reference frame is selected as illustrated in Fig. 1. For sake of clarity, in Fig. 1b, the coordinate system is translated along the positive x-direction by half tube length. Notice that, in both flows, x denotes the flow direction. In shear flow, y and z are the gradient and vorticity axes. The spherical particle, with diameter d_p, is located with center along the y-axis. For symmetry, the particle center remains on the plane $z = 0$ and only one half of the total geometry can be considered. Furthermore, the particle can only rotate around the z-axis. We denote the particle center by $\boldsymbol{x}_\mathrm{p} = (x_\mathrm{p}, y_\mathrm{p}, 0)$ and its rotation angle by θ_p. The volume occupied by the particle is $P(t)$ with boundary $\partial P(t)$. The particle moves in a domain Ω according to the imposed flow. We denote the particle translational and angular velocities by $\boldsymbol{u}_\mathrm{p} = (u_\mathrm{p}, v_\mathrm{p}, 0) = d\boldsymbol{x}_\mathrm{p}/dt$ and $\boldsymbol{\omega}_\mathrm{p} = \omega_\mathrm{p}\boldsymbol{k} = d\theta_\mathrm{p}/dt\,\boldsymbol{k}$, where $\boldsymbol{k}$ is the unit vector in the z-direction.

The dimensions of the domain in the shear flow case are L, H and $W/2$ along the x-, y- and z-axis, respectively; in Poiseuille flow, L and H are the tube length and diameter, and $W/2$ is the tube radius. The notation used for the external boundaries is illustrated in Fig. 1. In what follows, $\boldsymbol{n}$ indicates

the unit vector normal to a surface pointing from the fluid to a boundary, i.e., exiting the channel and entering the particle. Finally, in shear flow, the flow is generated by the motion of the boundaries Σ_{w} with velocity $\pm u_{\mathrm{w}}\boldsymbol{i}$, with u_{w} the magnitude of the wall velocity and $\boldsymbol{i}$ the unit vector denoting the x-direction. The imposed shear rate is, then, given by $\dot{\gamma} = 2u_{\mathrm{w}}/H$. In Poiseuille flow, a flow rate Q is imposed on the left boundary Σ_1.

Assuming inertialess conditions, the fluid dynamics is governed by the following mass and momentum balance equations

$$\nabla \cdot \boldsymbol{u} = 0 \tag{1}$$

$$\nabla \cdot \boldsymbol{\sigma} = \boldsymbol{0} \tag{2}$$

$$\boldsymbol{\sigma} = -p\boldsymbol{I} + 2\eta_{\mathrm{s}}\boldsymbol{D} + \boldsymbol{\tau} \tag{3}$$

where $\boldsymbol{\sigma}$, $\boldsymbol{u}$, p, $\boldsymbol{I}$, η_{s}, $\boldsymbol{D}$, and $\boldsymbol{\tau}$, are the total stress tensor, the velocity vector, the pressure, the 3×3 unity tensor, a Newtonian viscosity, the rate-of-deformation tensor $\boldsymbol{D} = (\nabla\boldsymbol{u} + (\nabla\boldsymbol{u})^{\mathrm{T}})/2$, and the viscoelastic stress tensor. We select the Giesekus constitutive equation [18] to model the viscoelastic fluid. According to this model, the viscoelastic stress tensor $\boldsymbol{\tau}$ is given by

$$\lambda \overset{\nabla}{\boldsymbol{\tau}} + \frac{\alpha\lambda}{\eta_{\mathrm{p}}}\boldsymbol{\tau} \cdot \boldsymbol{\tau} + \boldsymbol{\tau} = 2\eta_{\mathrm{p}}\boldsymbol{D} \tag{4}$$

where η_{p} is a constant viscosity, λ is the fluid relaxation time, and α is the so-called 'mobility parameter' [18] that modulates the shear-thinning behavior. The symbol $(\overset{\nabla}{})$ denotes the upper-convected time derivative, defined as

$$\overset{\nabla}{\boldsymbol{\tau}} \equiv \frac{\partial\boldsymbol{\tau}}{\partial t} + \boldsymbol{u} \cdot \nabla\boldsymbol{\tau} - (\nabla\boldsymbol{u})^{\mathrm{T}} \cdot \boldsymbol{\tau} - \boldsymbol{\tau} \cdot \nabla\boldsymbol{u} \tag{5}$$

A Newtonian fluid with constant viscosity $\eta_0 = \eta_{\mathrm{s}} + \eta_{\mathrm{p}}$ is obtained from Eqs. (3) and (4) by setting $\lambda = 0$.

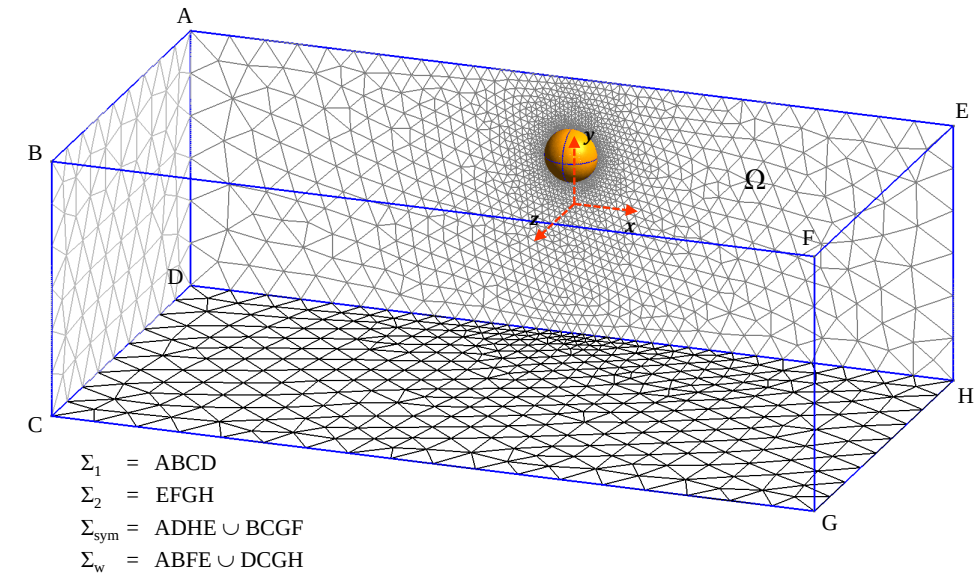

(a)

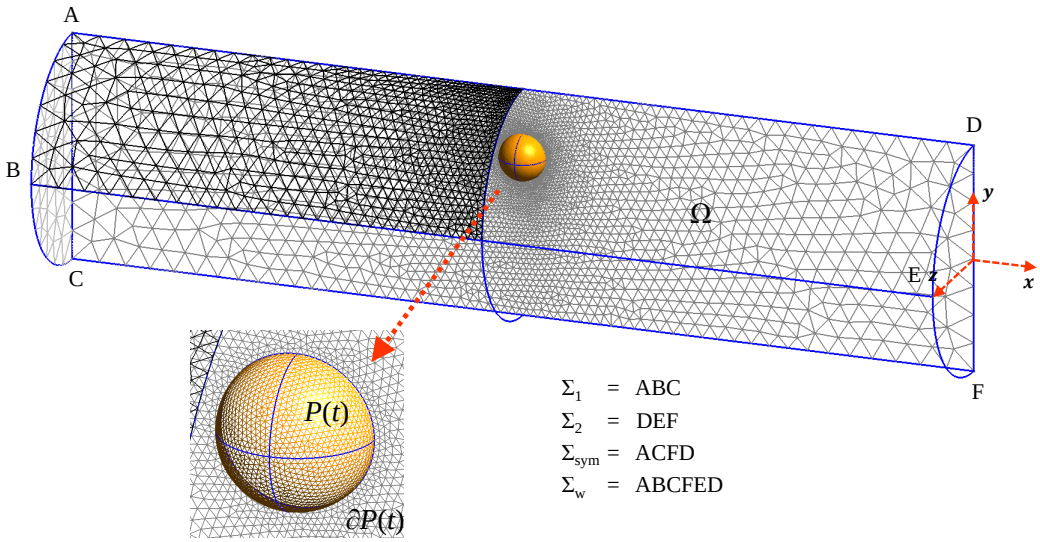

(b)

Figure 1: Computational domains and typical meshes used in shear (a) and Poiseuille (b) simulations. For sake of clarity, in (b) the coordinate system is translated along the positive x-direction by half tube length.

Concerning the boundary conditions, both problems have a symmetry plane corresponding to the plane $z = 0$. Furthermore, the plane at $z = W/2$ is also assumed to be a symmetry plane for the shear flow case. Hence, in both flows we have

$$\boldsymbol{u} \cdot \boldsymbol{n} = 0 \quad \text{on } \Sigma_{\text{sym}} \tag{6}$$

$$(\boldsymbol{\sigma} \cdot \boldsymbol{n})|_x = (\boldsymbol{\sigma} \cdot \boldsymbol{n})|_y = 0 \quad \text{on } \Sigma_{\text{sym}} \tag{7}$$

As mentioned above, in shear flow, the upper and lower walls are moved with velocity $\boldsymbol{u}_{\text{w}} = (\pm\, u_{\text{w}}, 0, 0)$. However, since slip occurs at these walls, only the normal components of the fluid velocity $\boldsymbol{u}$ and the wall velocity $\boldsymbol{u}_{\text{w}}$ are equal at the wall surface. Regarding the tangential components, we use the Navier slip boundary condition that linearly relates the tangential component of the traction on the fluid and the tangential component of the difference between the fluid and the solid velocities. Therefore, we have

$$\boldsymbol{u} \cdot \boldsymbol{n} = \boldsymbol{u}_{\text{w}} \cdot \boldsymbol{n} \quad \text{on } \Sigma_{\text{w}} \tag{8}$$

$$(\boldsymbol{I} - \boldsymbol{n}\boldsymbol{n}) \cdot (\boldsymbol{\sigma} \cdot \boldsymbol{n}) = -\frac{\eta_0}{\lambda_{\text{w}}} (\boldsymbol{I} - \boldsymbol{n}\boldsymbol{n}) \cdot (\boldsymbol{u} - \boldsymbol{u}_{\text{w}}) \quad \text{on } \Sigma_{\text{w}} \tag{9}$$

where $\boldsymbol{I} - \boldsymbol{n}\boldsymbol{n}$ is the tangential projection operator and λ_{w} is the wall slip parameter. Since λ_{w} has the dimension of a length, it is often called the 'slip length'. Notice that the slip length λ_{w} can be interpreted as the fictitious distance beyond the wall such that the linearly extrapolated velocity profile would satisfy the no-slip boundary condition, i.e., where the fluid would have the same velocity of the wall. Finally, periodicity is applied for the velocity

and the traction between the left and right boundaries:

$$\boldsymbol{u}|_{\Sigma_1} = \boldsymbol{u}|_{\Sigma_2} \tag{10}$$

$$-(\boldsymbol{\sigma}\cdot\boldsymbol{n})|_{\Sigma_1} = (\boldsymbol{\sigma}\cdot\boldsymbol{n})|_{\Sigma_2} \tag{11}$$

In Poiseuille flow, the slip condition at the fixed wall is

$$\boldsymbol{u}\cdot\boldsymbol{n} = \boldsymbol{0} \quad \text{on } \Sigma_{\mathrm{w}} \tag{12}$$

$$(\boldsymbol{I}-\boldsymbol{n}\boldsymbol{n})\cdot(\boldsymbol{\sigma}\cdot\boldsymbol{n}) = -\frac{\eta_0}{\lambda_{\mathrm{w}}}(\boldsymbol{I}-\boldsymbol{n}\boldsymbol{n})\cdot\boldsymbol{u} \quad \text{on } \Sigma_{\mathrm{w}} \tag{13}$$

Periodicity is imposed between the inflow and outflow boundaries

$$\boldsymbol{u}|_{\Sigma_1} = \boldsymbol{u}|_{\Sigma_2} \tag{14}$$

$$(\boldsymbol{\sigma}\cdot\boldsymbol{i})|_{\Sigma_1} = (\boldsymbol{\sigma}\cdot\boldsymbol{i})|_{\Sigma_2} - \Delta p\,\boldsymbol{i} \tag{15}$$

$$-\int_{\Sigma_1}\boldsymbol{u}\cdot\boldsymbol{n}\,dS = Q \tag{16}$$

where Δp is the pressure drop along the tube (in between Σ_1 and Σ_2). The flow rate in Eq. (16) is imposed through a constraint where the associated Lagrange multiplier is identified as the unknown pressure difference Δp [19].

Finally, adherence is assumed on the particle surface $\partial P(t)$ resulting in the rigid-body motion equation

$$\boldsymbol{u} = \boldsymbol{u}_{\mathrm{p}} + \boldsymbol{\omega}_{\mathrm{p}}\times(\boldsymbol{x}-\boldsymbol{x}_{\mathrm{p}}) \quad \text{on } \partial P(t) \tag{17}$$

To close the set of equations, the hydrodynamic force and torque acting on the particle need to be specified. Under the assumptions of no 'external' forces and torques, and inertialess particle, such balance equations are given by

$$\boldsymbol{F} = \int_{\partial P(t)}\boldsymbol{\sigma}\cdot\boldsymbol{n}\,dS = \boldsymbol{0} \tag{18}$$

$$\boldsymbol{T} = \int_{\partial P(t)}(\boldsymbol{x}-\boldsymbol{x}_{\mathrm{p}})\times(\boldsymbol{\sigma}\cdot\boldsymbol{n})\,dS = \boldsymbol{0} \tag{19}$$

where $\boldsymbol{F} = (F_{\mathrm{x}}, F_{\mathrm{y}}, 0)$ and $\boldsymbol{T} = T\boldsymbol{k}$ are the total force and torque on the particle boundary $\partial P(t)$.

An initial condition for the stress tensor is also needed. We set

$$\boldsymbol{\tau}|_{t=0} = \mathbf{0} \tag{20}$$

corresponding to a stress-free state in the whole fluid domain.

Once the fluid velocity, pressure and stress fields are calculated along with the particle kinematic quantities, the particle position and rotation are updated by integrating the following equations

$$\frac{d\boldsymbol{x}_{\mathrm{p}}}{dt} = \boldsymbol{u}_{\mathrm{p}} \tag{21}$$

$$\frac{d\theta_{\mathrm{p}}}{dt} = \omega_{\mathrm{p}} \tag{22}$$

with initial conditions $\boldsymbol{x}_{\mathrm{p}}|_{t=0} = (0, y_{\mathrm{p},0}, 0)$ and $\theta_{\mathrm{p}}|_{t=0} = \theta_{\mathrm{p},0}$.

The governing equations are made dimensionless by choosing, for the shear flow problem, the gap H as characteristic length, $\dot{\gamma}H$ as characteristic velocity, and $\eta_0\dot{\gamma}$ as characteristic stress. In Poiseuille flow, we select the tube diameter H as characteristic length, $\bar{u} = 4Q/(\pi H^2)$ as characteristic velocity and $\eta_0\bar{u}/H$ as characteristic stress. In both cases, the characteristic time t_{f} is defined as the ratio between characteristic length and velocity, i.e., $t_{\mathrm{f}} = 1/\dot{\gamma}$ in shear and $t_{\mathrm{f}} = \pi H^3/(4Q)$ in Poiseuille flow. Then, the following dimensionless parameters appear in the governing equations: the confinement ratio $\beta = d_{\mathrm{p}}/H$, the wall slip coefficient λ_{w}/H, the Deborah number $De = \lambda/t_{\mathrm{f}}$, the viscosity ratio η_{s}/η_0, and the constitutive parameter α. In what follows, all the symbols will refer to dimensionless quantities.

3. Numerical method and code validation

3.1. Numerical method

The governing equations are solved by means of the finite element method. The particle motion is handled through the Arbitrary Lagrangian-Eulerian (ALE) approach [20]. As previously done [8, 17], at each time step the mesh is rigidly translated along the flow direction by a velocity equal to the particle translational velocity. In this way, mesh distortion only occurs along the migration direction, preserving a sufficient accuracy during the whole simulation without needing to remesh.

The continuity and momentum balance equations are decoupled from the constitutive equation [21]. An implicit-stress formulation is used for the momentum balance discretization whereby the viscoelastic stress tensor term is replaced by the space-continuous but time-discretized form of the constitutive equation through an Euler scheme implicit in the velocity [22]. Finally, the constitutive equation is discretized through a semi-implicit Gear scheme, and the Streamline-Upwind/Petrov-Galerkin (SUPG) technique [23] with a log-representation for the 'conformation tensor' [24, 25] are used to stabilize the code. The force- and torque-free conditions are imposed through Lagrange multipliers in each node of the spherical surface. The particle kinematic quantities are included as additional unknowns and are computed from the solution of the governing equations [8].

Further details on the implementation, the weak form and the adopted solver can be found elsewhere [8].

3.2. Code validation

Mesh and time convergence are checked for all the simulations reported in this work. A typical mesh used in the simulations is illustrated in Fig. 1. In this figure, only the element distribution on three faces and on the spherical surface is shown. The domain is discretized through tetrahedral elements refined around the particle where the largest gradients are expected. A continuous quadratic interpolation for the velocity, a continuous linear interpolation for pressure, and a continuous linear interpolation for the stress tensor are used [8]. To avoid any artificial effect on the particle dynamics due to the periodic boundary conditions, the length of the computational domain in the x-direction is selected sufficiently larger than the particle diameter. The same criterion is adopted to set the depth $W/2$ of the domain in shear flow. We get $L/d_\mathrm{p} = W/d_\mathrm{p} = 15$ in shear flow and $L/d_\mathrm{p} = 20$ in Poiseuille flow.

Figure 2 shows a typical convergence test for shear (a) and Poiseuille (b) flows. In these plots, the particle migration velocity v_p is reported as function of time t for different mesh resolutions (see Table 1) and time step sizes. The fair superposition of the data indicates that, for the chosen parameters, both mesh and time convergence are satisfied.

For all the simulations, a mesh with 80 elements on the particle equator satisfies mesh convergence. In both flows, however, an extra refinement between the particle and the closest boundary is needed when the particle starts quite close to the wall (e.g., $y_{\mathrm{p},0} = 0.35$). Therefore, the total number of elements varies from about 40,000 to 50,000 in shear flow and from 70,000 to 90,000 in Poiseuille flow. Finally, a time step $\Delta t = 0.01$ is sufficient to achieve time convergence.

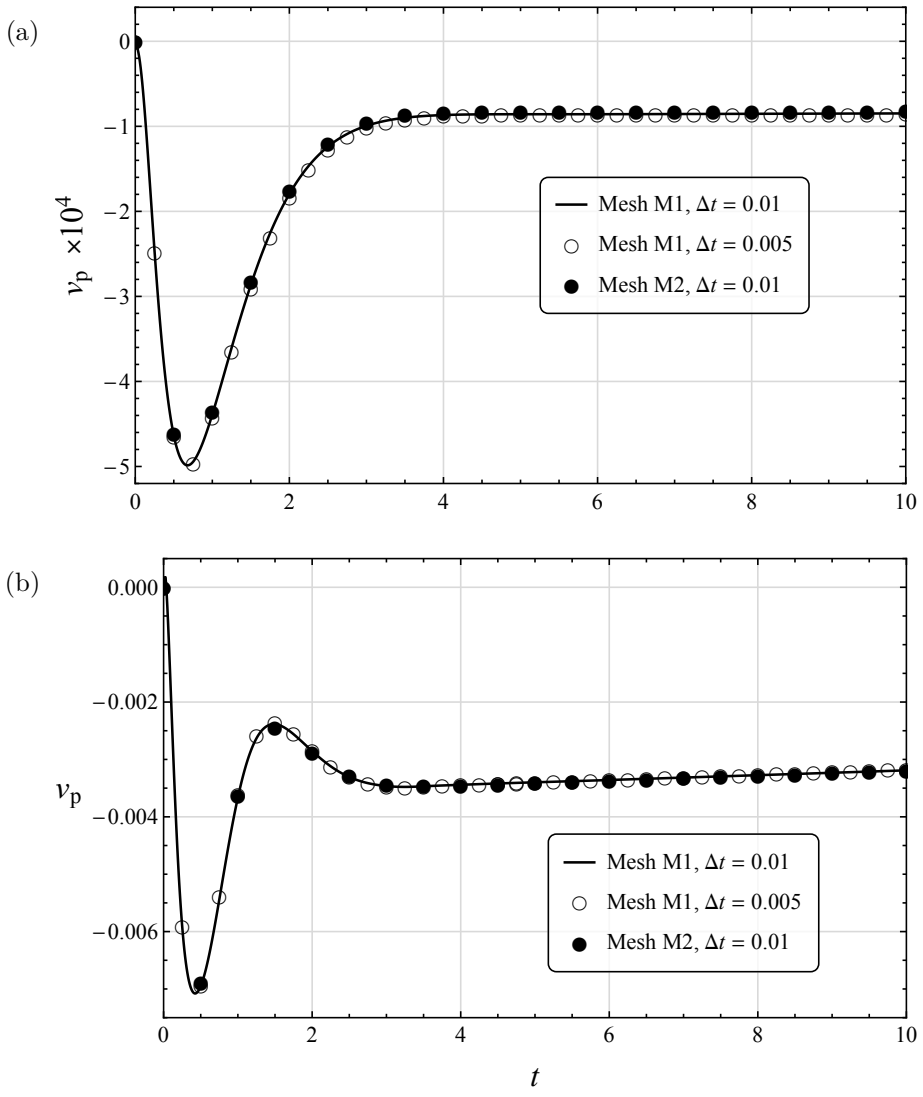

Figure 2: Particle migration velocity v_p for different mesh resolutions (see Table 1) and time step sizes. (a) shear flow with $y_{\mathrm{p},0} = 0.35$ and $\lambda_\mathrm{w} = 0.5$; (b) Poiseuille flow with $y_{\mathrm{p},0} = 0.2$ and $\lambda_\mathrm{w} = 0.1$. The other parameters are: $De = 1.0$, $\alpha = 0.2$, $\eta_\mathrm{s}/\eta_0 = 0.091$, and $\beta = 0.2$.

Mesh label	M1	M2	M1	M2
Particle y-position	0.20	0.20	0.35	0.35
Shear				
#el. on the particle equator	80	100	80	100
#el. in the mesh	42,210	67,061	49,505	82,610
Poiseuille				
#el. on the particle equator	80	90	80	100
#el. in the mesh	68,667	104,746	92,082	113,566

Table 1: Parameters of the meshes used in the simulation results shown in Fig. 2.

4. Results

In this section, we present simulation results for the dynamics of a spherical particle suspended in a fluid subjected to a confined shear or Poiseuille flow with slip on the channel walls. The wall slip coefficient λ_{w} is varied in the range $[10^{-3} - 1]$; the other parameters are kept fixed to the following values: $\alpha = 0.2$, $\beta = 0.2$, $De = 1.0$, $\eta_{\mathrm{s}}/\eta_0 = 0.091$. (Notice that the non-zero value of the constitutive parameter α denotes a shear-thinning fluid.) We choose this set of values to allow a direct comparison with our previous works on migration in viscoelastic fluids with no-slip conditions [8, 6] and with slip on the particle surface [17].

For a fixed set of parameters, simulations are carried out by placing the particle at different positions along the channel gap. Following previous works [8, 17], we report the particle kinematic quantities in terms of 'mastercurves', i.e., the trends of the particle translational and angular velocities as a function

of the actual position of the particle center of volume, after the 'fast' initial transients due to the viscoelastic stress building-up have extinguished. Due to the symmetry, only the curves corresponding to the 'upper-half' of the channel are shown, i.e., from $y = 0$ (the channel centerline) to $y = 0.4$ (the distance from the wall corresponding to a particle radius). In the following figures, the data obtained from the simulations are shown as symbols. The lines passing through the symbols are interpolating curves that are added in the plots just as guides to the eye. In the case of a viscoelastic suspending medium and for high slip coefficients, numerical issues prevent the calculation of the particle dynamics very close to the wall. As previously done [17], we extrapolate the mastercurve toward the wall when the value of a specific kinematic quantity is known at the wall (e.g., the migration velocity must become zero when the particle touches the wall). If this is not the case, the interpolation is limited within the data range.

4.1. Shear flow

We first analyze the shear flow case. To better understand the simulation results, it is worthwhile recalling that, in this kind of flow, for both Newtonian and viscoelastic fluids, the effect of wall slip on the fluid without particles is that of reducing the fluid shear rate with respect to the no-slip case, while the velocity profile remains linear. We denote with $\dot{\gamma}_{\mathrm{eff}}$ the shear rate in a confined fluid without particles where slip occurs at the walls. Of course, $\dot{\gamma}_{\mathrm{eff}}$ depends on the slip coefficient and the fluid rheological properties.

In Fig. 3, we report the difference between the x-component of the particle translational velocity u_{p} and the undisturbed local fluid flow velocity $u_0 = \dot{\gamma}_{\mathrm{eff}}\, y_{\mathrm{p}}$ as a function of the particle position y_{p}, for different slip coefficients λ_{w}.

This relative velocity is also known as 'slip velocity' [26], but it has nothing to do with the slip boundary condition at the wall. The solid lines refer to the viscoelastic case for six values of the slip coefficient. The no-slip case is shown as a black solid line that is hardly visible since it is below the orange one. Finally, the dashed lines correspond to the Newtonian fluid for the no-slip case (black) and for the highest slip coefficient (red).

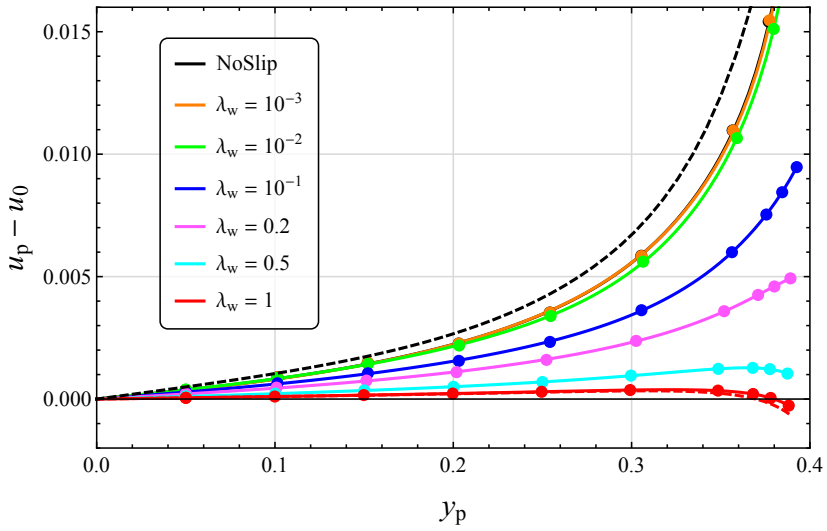

Figure 3: Difference between the x-component of the particle translational velocity $u_p(y_p)$ and the local undisturbed fluid flow velocity $u_0(y_p) = \dot{\gamma}_{eff}\, y_p$ as a function of the particle position y_p, for different slip coefficients λ_w in shear flow. A Newtonian (dashed lines) and a viscoelastic (solid lines) suspending fluids are considered. The black lines refer to the no-slip case.

First of all, it can be observed that, for slip coefficients up to $\lambda_w = 0.2$, the slip velocity is positive (i.e., the particle 'leads' the fluid) and it increases as the particle moves toward the wall. This relative velocity progressively reduces for increasing values of λ_w, due to the corresponding reduction of the fluid velocity. However, for sufficiently high λ_w-values, the trend close to

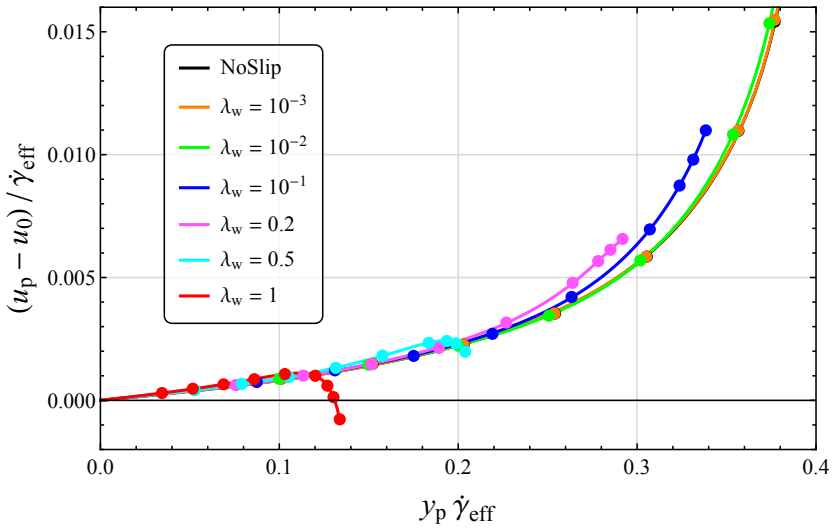

Figure 4: Viscoelastic data of Fig. 3 scaled through the effective shear rate $\dot{\gamma}_{\text{eff}}$, which is a function of the slip coefficients λ_w.

the wall changes: indeed, starting from $\lambda_w = 0.5$ the slip velocity exhibits a maximum and, at $\lambda_w = 1.0$, it even changes sign, for both Newtonian and viscoelastic fluids. This behavior observed for particles very close to the wall is in agreement with the results of Luo and Pozrikidis [15] for a Newtonian sheared fluid, and is due to the influence of the particle-wall hydrodynamic interactions on the slip boundary condition. In fact, due to the presence of the particle, the stress on the wall is modified and, consequently, the fluid velocity is different from the undisturbed case (that is the velocity u_0 used to calculate the slip velocity). Finally, when comparing the Newtonian and viscoelastic curves, a slight deviation is observed for the no-slip case (dashed black line and solid black line), whereas the curves coincide for the largest λ_w-value (dashed and solid red lines).

Since wall slip reduces the shear rate $\dot{\gamma}_{\text{eff}}$ of the undisturbed flow, the

difference between particle and fluid velocities decreases as well. The fair superposition of the data in Fig. 4 demonstrates that the slip velocity can be rescaled through the effective shear rate. In the Newtonian case, the effective shear rate is given by $1/(1 + 2\lambda_w)$. In the viscoelastic case, it has been computed by numerically solving the governing equations for a viscoelastic fluid in a channel with slip boundary conditions at the walls. Because the undisturbed shear flow with slip on the wall corresponds to a no-slip flow in a wider channel (remember the interpretation of the slip length), also the characteristic length has to be rescaled; then, the wall 'moves' from 0.4 in the no-slip case to $0.4\dot{\gamma}_{\text{eff}}$ when slip is present. The scaled data in Fig. 4 show that the no-slip behavior is recovered in a wide region of the channel, except close to the wall due to the reason mentioned above.

Figure 5 shows the difference between the particle angular velocity and one-half of the effective shear rate for a Newtonian (Fig. 5a) and a viscoelastic (Fig. 5b) suspending liquid. Notice that the quantity $\dot{\gamma}_{\text{eff}}/2$ is the rotation rate of a particle in an unbounded shear flow with shear rate given by $\dot{\gamma}_{\text{eff}}$.

The shear flow induces a clockwise particle rotation (as seen from the z-axis) corresponding to a negative angular velocity; thus, positive values of the angular velocity difference indicate that the confinement slows down the particle rotation. The data reported in these figures show, for a fixed value of the slip coefficient, a monotonic increasing trend as the particle moves from the midplane to the wall (i.e., the angular velocity slows down more and more). Notice also that the scale of the angular velocity axis for a viscoelastic suspending medium (Fig. 5b) covers a wider range as compared to Newtonian case (Fig. 5a). Hence, in agreement with the previous literature [27, 8], both

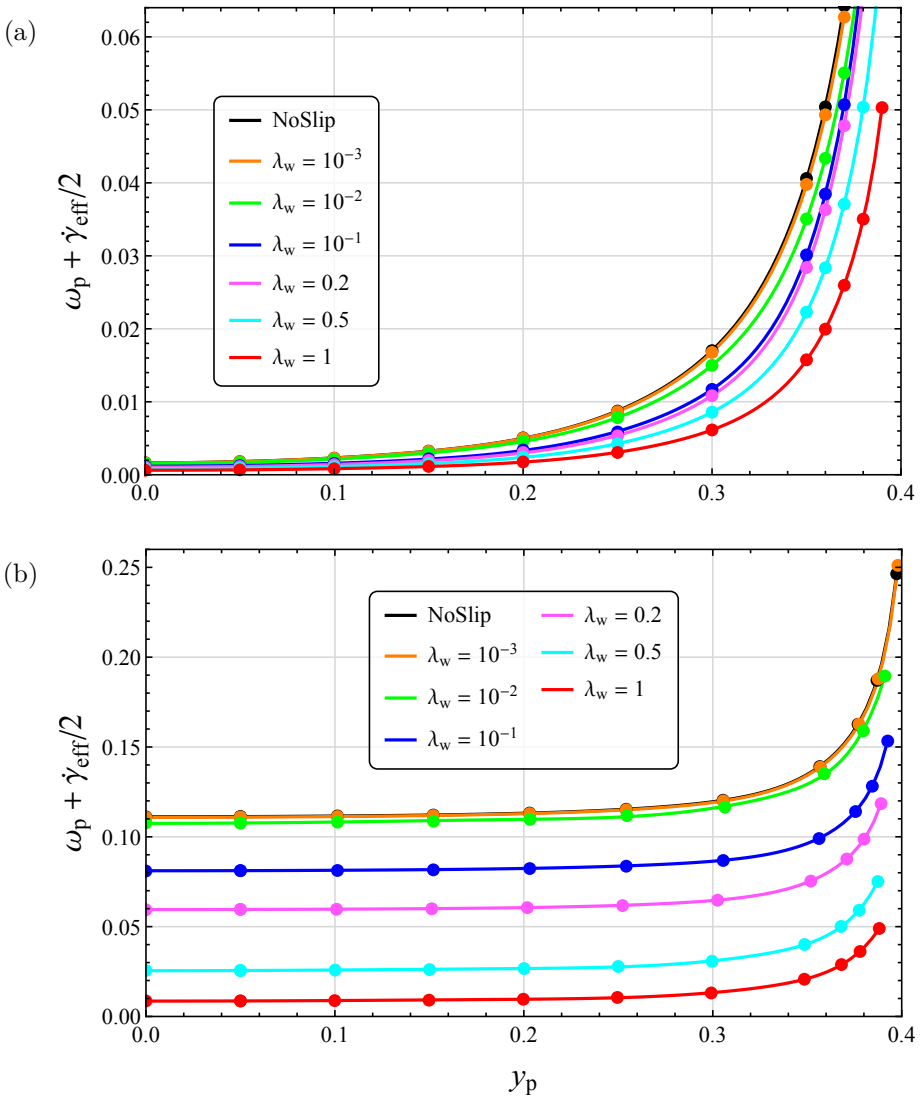

Figure 5: Difference between the particle angular velocity $\omega_p(y_p)$ and one-half of the effective shear rate $\dot{\gamma}_{eff}(\lambda_w)$ as a function of the particle position y_p for different slip coefficients λ_w in shear flow, for a Newtonian (a) and a viscoelastic (b) suspending fluid. The black lines refer to the no-slip case.

confinement and fluid viscoelasticity slow down the particle rotation. On the other hand, although the effective shear rate decreases (in modulus) with growing slip and the particle angular velocity decreases accordingly, their difference (that is the quantity reported on the y-axis of Fig. 5) also decreases. Therefore, for both suspending fluids, increasing values of the wall slip coefficient slow down the particle rotation but increase its 'normalized' value $\omega_\mathrm{p} + \dot{\gamma}_\mathrm{eff}/2$. In other words, for increasing wall slip, a particle in a confined sheared suspension rotates faster than the same particle suspended in an unconfined sheared fluid with shear rate equal to the effective shear rate of the confined system.

Finally, the effect of wall slip on the migration phenomenon is illustrated in Fig. 6a, where the migration velocity of the particle v_p is shown as function of its position y_p, for different values of the slip coefficient λ_w. Notice that a positive v_p indicates a particle moving toward the wall, whereas a negative value implies a migration toward the channel midplane. We recall that a particle suspended in a sheared viscoelastic fluid with no-slip at the fluid-solid interfaces or with slip on the particle surface migrates toward the closest wall regardless of its initial position [8, 17]. As depicted in Fig. 6a, slip at the fluid-wall interface changes such a scenario. For small values of the slip coefficient (up to $\lambda_\mathrm{w} = 0.1$, blue curve in Fig. 6a), the mastercurves are qualitatively similar to those corresponding to the no-slip case. Indeed, the migration velocity is always positive, increasing as the particle moves from the channel midplane toward the wall up to reaching a maximum, and then steeply decreasing to zero when the particle approaches the wall. In this range, slip only slows down the migration velocity. On the other hand, for $\lambda_\mathrm{w} = 0.2$

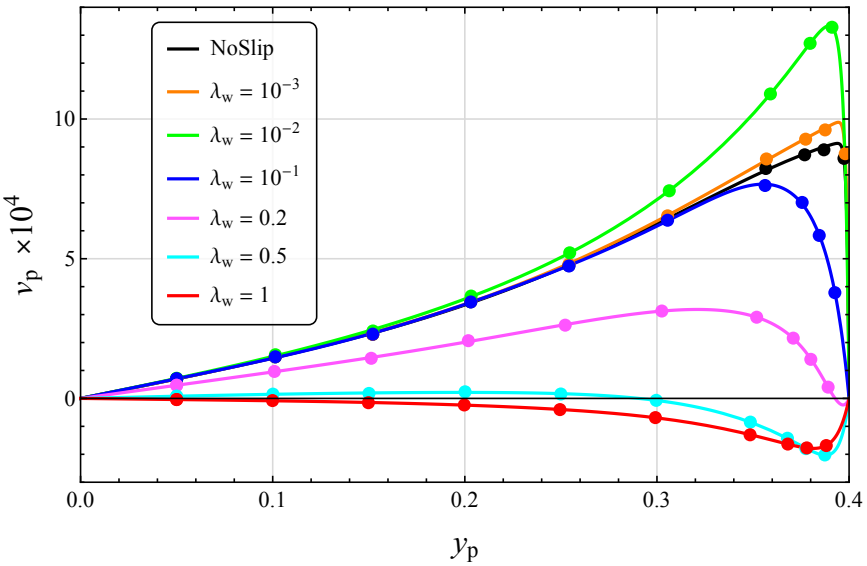

(a)

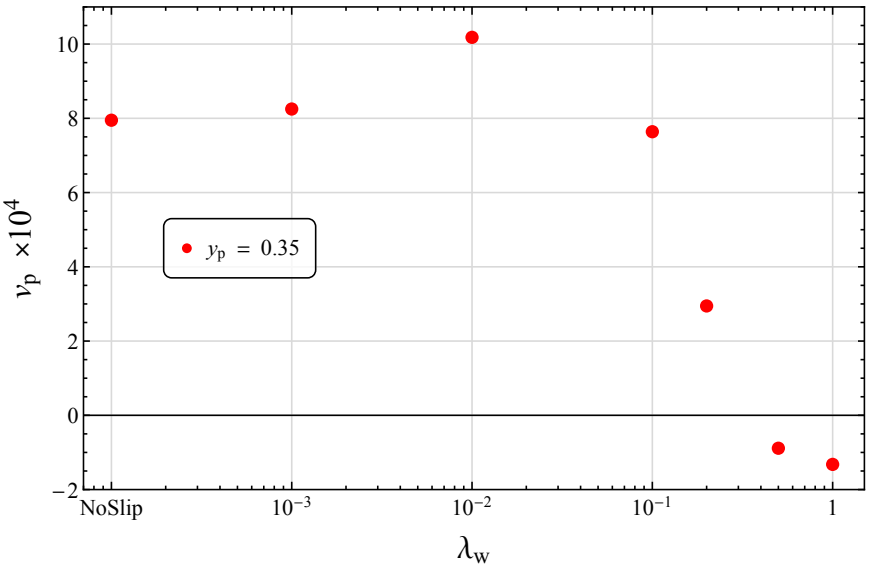

(b)

Figure 6: (a) Migration velocity $v_p(y_p)$ of the particle as a function of its position y_p, for different slip coefficients λ_w in shear flow. Only the case with a viscoelastic suspending fluid is considered. The black line refers to the no-slip case. (b) Migration velocity of the particle v_p as a function of the slip coefficients λ_w for $y_p = 0.35$.

and $\lambda_w = 0.5$, the migration velocity is still positive near the midplane but becomes negative near the wall. Hence, the wall becomes repulsive and an intermediate equilibrium position appears corresponding to the intersection of the mastercurves and the x-axis of the diagram. Such an equilibrium position moves toward the channel midplane as the slip coefficient increases. This behavior further changes for the highest value of the slip coefficient investigated in this work ($\lambda_w = 1$, red curve in Fig. 6a), where the migration velocity is negative for any position through the channel, i.e., all the particles move to the axis.

To better clarify the effect of wall slip, we show in Fig. 6b the migration velocity as a function of the slip coefficient for a fixed particle position $y_p = 0.35$. A non-monotonic trend of v_p is observed as the slip coefficient increases. For small λ_w-values, the migration velocity initially grows, reaches a maximum around $\lambda_w = 10^{-2}$ (corresponding to the green curve in Fig. 6a), then it progressively decreases. At high values of the slip coefficient, v_p becomes negative, with consequent inversion of the migration direction.

To summarize, depending on the slip coefficient, the migration velocity under shear flow with slip on the wall can be higher or lower (in magnitude) than the no-slip case. The migration direction is toward: (i) the closest wall for $\lambda_w \lesssim 0.1$, (ii) an intermediate equilibrium position for $\lambda_w \approx 0.5$, (iii) the midplane for $\lambda_w \gtrsim 1$.

The presence of this equilibrium position can be also visualized through the time evolution of the particle position $y_p(t)$ (i.e., the particle trajectories along the channel gap) reported in Fig. 7. Two starting points are considered, one close to the center ($y_{p,0} = 0.1$) and one close to the wall ($y_{p,0} = 0.3$). The

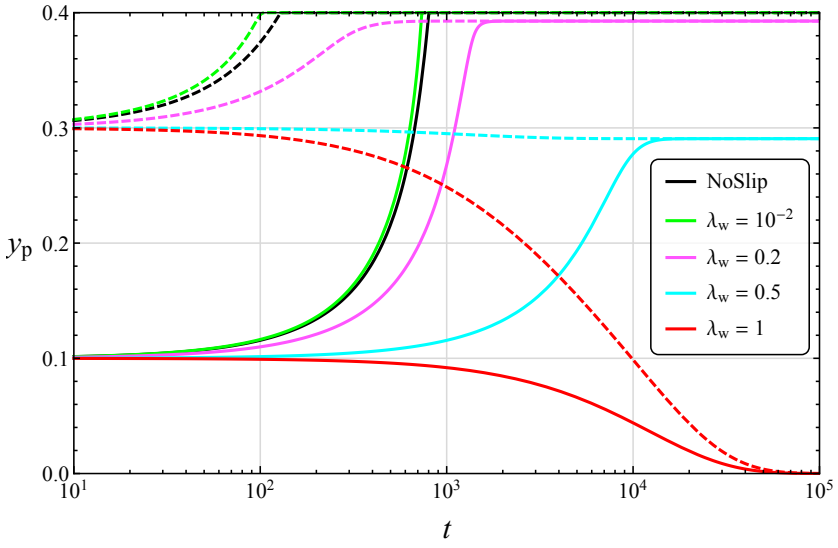

Figure 7: Particle position y_p as function of time t for two initial positions $y_{p,0} = 0.1$ (solid lines) and $y_{p,0} = 0.3$ (dashed lines), and for different slip coefficients λ_w in shear flow.

fast initial transient phase is not shown. At low λ_w-values, all the particles migrate toward the wall (black and green curves). Starting from $\lambda_w = 0.2$ (magenta) the wall becomes an unstable equilibrium position and the particles migrate toward an intermediate equilibrium position that, however, is very close to the wall. This equilibrium position moves toward the channel center as the slip coefficient increases (it is around 0.3 for $\lambda_w = 0.5$ (cyan)). Finally, the equilibrium position becomes the channel midplane for $\lambda_w = 1$ (red).

4.2. Poiseuille flow

Let us now consider the case of Poiseuille flow with slip on the wall. In this kind of flow, the undisturbed velocity profile becomes more and more plug-flow-like as the slip increases for both Newtonian and viscoelastic fluids. In particular, the Newtonian dimensionless velocity profile can be seen as

the composition of a parabolic profile with average velocity $1/(1+8\lambda_w)$ and a plug flow (total slip) with (constant) velocity of the slipping fluid at the wall $8\lambda_w/(1+8\lambda_w)$. These coefficients have been calculated by solving the governing equations for a Newtonian fluid in a tube with the slip boundary condition at the wall.

Figures 8a and 8b show the velocity difference $u_p - u_0$ (the slip velocity) in the Newtonian and viscoelastic case, respectively, as a function of the particle radial position and for different slip coefficients. In both suspending fluids, the slip velocity is negative at any position through the channel and for any value of λ_w, i.e., the particle always 'lags' the fluid. Furthermore, its absolute value increases as the particle-wall distance is reduced, except for $\lambda_w = 1$ where an opposite trend is observed very close to the wall.

Similarly to the shear flow case, the modulus of the slip velocity is progressively reduced as the slip coefficient is increased. In particular, for the largest value of λ_w investigated (red curves), the particle translational velocity approximately coincides with the undisturbed fluid velocity. In this case, the fluid velocity profile is flat far from the sphere and the particle dynamics becomes similar to that of a freely suspended sphere in a medium with uniform far-field velocity, where the particle translates at the same velocity of the fluid. The effect of a flat profile is even more evident for the viscoelastic case (Fig. 8b). Due to the fluid shear-thinning, the velocity profile is flatter near the tube axis and steeper close to the wall as compared to the Newtonian case. Consequently, the slip velocity $u_p - u_0$ is lower around the channel axis and higher close to the wall.

The trends of the particle angular velocity are reported in Fig. 9 for

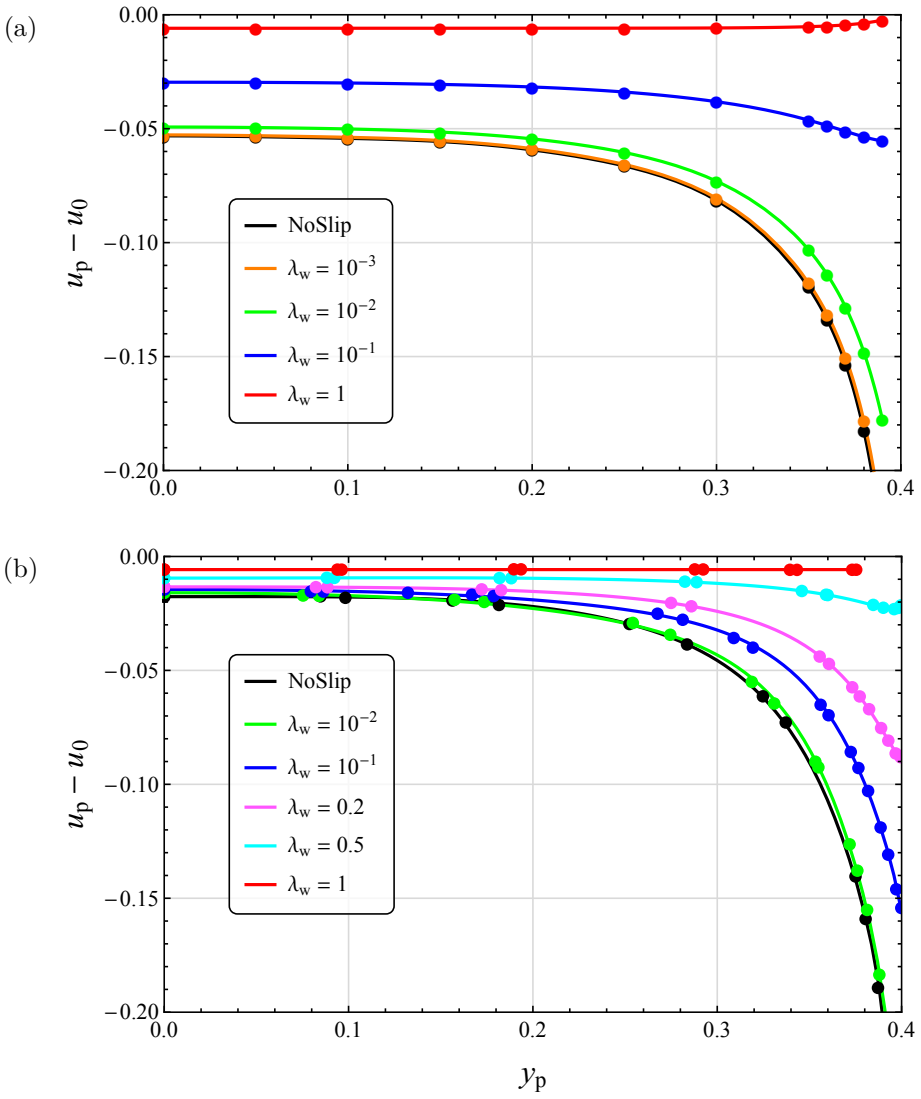

Figure 8: Difference between the x-component of the particle translational velocity u_p and the local undisturbed fluid flow velocity u_0 as a function of the particle position y_p, for different slip coefficients λ_w in Poiseuille flow. A Newtonian (a) and a viscoelastic (b) suspending fluids are considered. The black lines refer to the no-slip case.

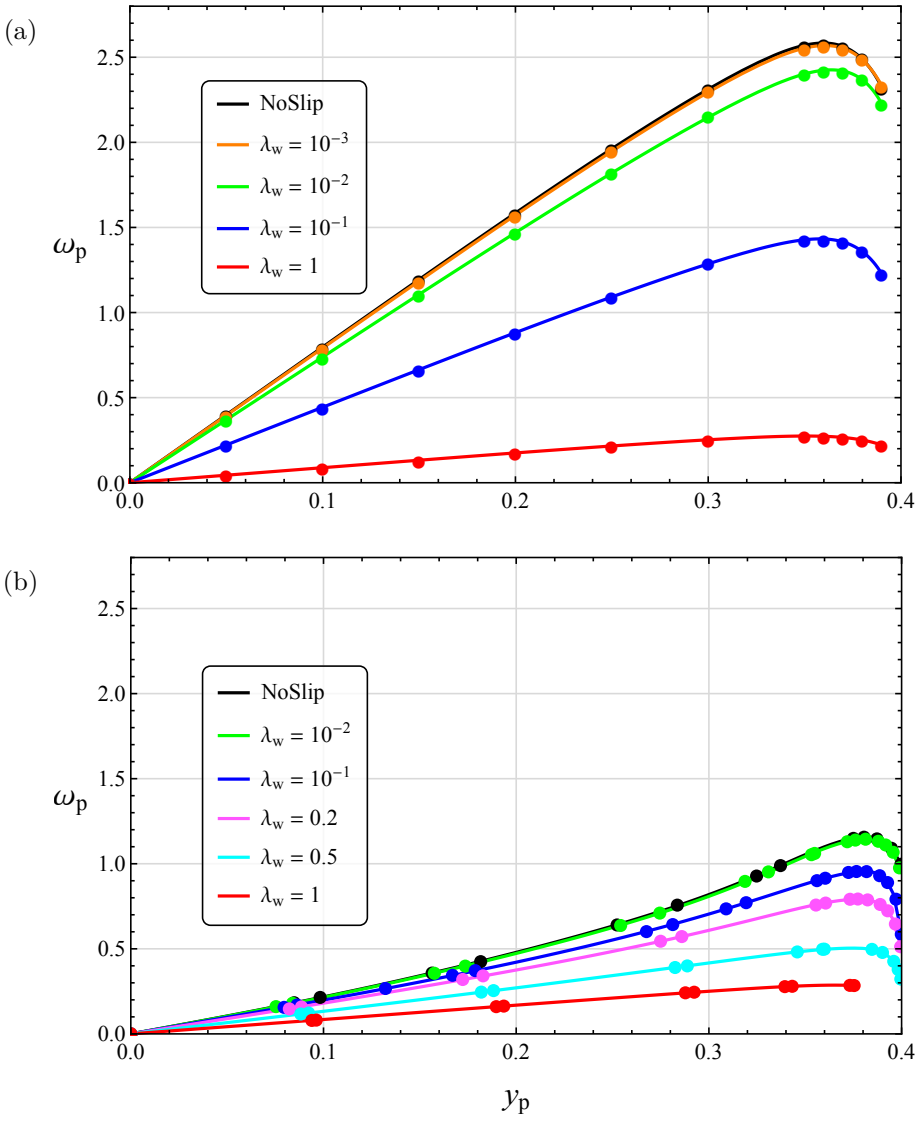

Figure 9: Particle angular velocity ω_p as a function of the particle position y_p, for different slip coefficients λ_w in Poiseuille flow. A Newtonian (a) and a viscoelastic (b) suspending fluids are considered. The black lines refer to the no-slip case.

both the Newtonian and viscoelastic cases. In the Newtonian case, ω_p grows linearly moving from the axis to the wall, reaches a maximum near the wall and tends to a finite value as the particle approaches the wall. In the viscoelastic case, ω_p has a similar behavior although it is always lower in magnitude as compared to the Newtonian case, i.e., viscoelasticity slows down the particle rotation. As the slip velocity, the angular velocity depends on the local shear rate, decreasing with growing λ_w. Thus, in both cases, the angular velocity is progressively reduced as the slip coefficient is increased. In the limit of total slip (flat velocity profile), the particle does not rotate.

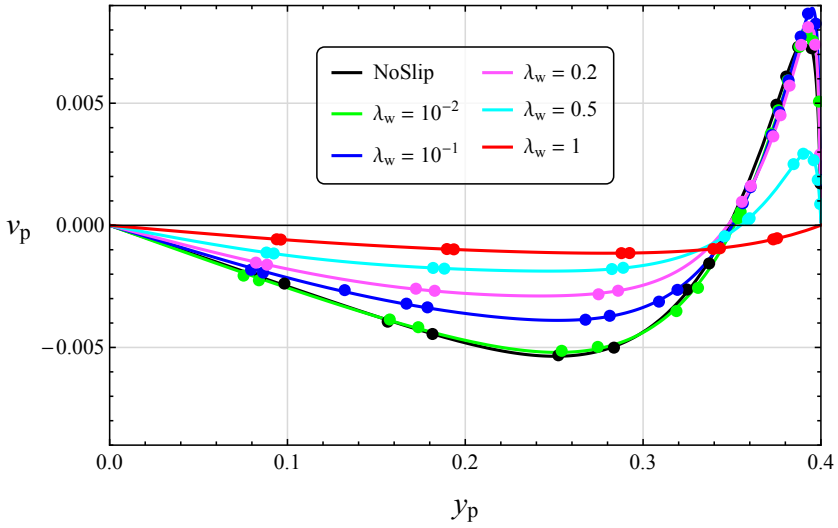

Figure 10: Migration velocity of the particle v_p as a function of its position y_p in Poiseuille flow for different wall slip coefficients λ_w. A viscoelastic suspending fluid is considered. The black line refers to the no-slip case.

Finally, in Figs. 10 and 11, the mastercurves of the particle migration velocity and some trajectories for different values of the wall slip coefficient are shown, respectively. Let us first consider the no-slip case (black lines in the

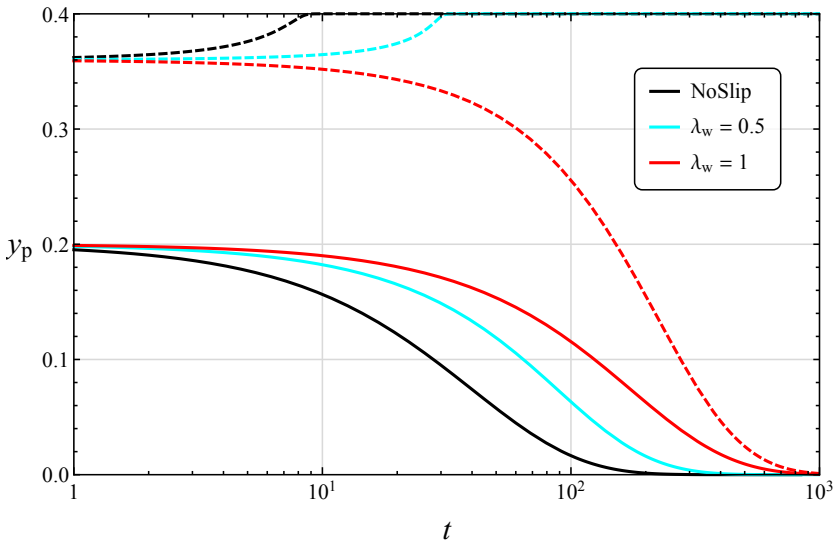

Figure 11: Particle position y_p as function of time t for two initial positions $y_{p,0} = 0.2$ (solid lines) and $y_{p,0} = 0.36$ (dashed lines), and for different slip coefficients λ_w in Poiseuille flow.

two figures). In agreement with previous works (see, e.g., [6]), the migration velocity is negative for a particle located between the channel centerline and a 'critical' equilibrium position y_N (≈ 0.35 for the chosen set of parameters), and is positive between y_N and the wall. Therefore, as shown in Fig. 11, the particle migrates toward the channel centerline for $0 < y_p < y_N$ or the wall for $y_p > y_N$, i.e., y_N is an unstable equilibrium position.

Up to $\lambda_w = 0.5$ (cyan curve in Fig. 10), the mastercurves are qualitatively similar to the no-slip case. On the other hand, by further increasing the slip coefficient, the migration dynamics qualitatively changes. Indeed, at $\lambda_w = 1$ (red curves), the migration velocity is negative for any position of the particle through the channel. Therefore, the unstable equilibrium position disappears, the wall becomes repulsive, and the migration direction is always toward the channel centerline. This behavior is readily visible Fig. 11 where both the red curves tend to the channel centerline. Finally, notice that the magnitude of the migration velocity decreases as the slip coefficient increases. Indeed, the flattening of the velocity profile at high λ_w-values reduces the fluid normal stress gradient, weakening the migration phenomenon.

In conclusion, similarly to the case of slip on the particle-fluid interface (see [17]), fluid viscoelasticity combined with a sufficiently large slip at the channel wall drives the suspended particles toward the channel centerline regardless of their starting position. On the other hand, wall slip reduces the shear rate gradients through the channel, slowing down the migration dynamics.

5. Conclusions

We investigated the effect of wall slip on the dynamics of a single, rigid sphere in a Newtonian and viscoelastic shear-thinning fluid under shear and Poiseuille flows through 3D direct finite element simulations with an ALE formulation to handle the particle motion.

In both flow fields, the particle translational velocity along the flow direction approaches the velocity of the unperturbed fluid as the wall slip coefficient increases. Furthermore, higher slip coefficients slow down the particle rotation due to the reduction of the effective shear rate in shear flow and the flattening of the velocity profile in Poiseuille flow. In a viscoelastic fluid, wall slip qualitatively changes the migration dynamics in both flow fields as compared to the no-slip case. In shear flow, sufficiently high slip coefficients reverse the migration direction, making the wall an unstable equilibrium position and driving all the particles toward the channel midplane. It is worthwhile to mention that this behavior is at variance with the no-slip case as well as the case of slip on the particle-fluid interface where the migration direction is always toward the wall. Similarly, in Poiseuille flow, the tube wall becomes an unstable equilibrium position, and the particles migrate toward the channel centerline regardless of their position. In both flow fields, however, the magnitude of the migration velocity is reduced. Hence, slip effects must be properly taken into account when designing 3D focusing microdevices.

References

[1] G. M. Whitesides, The origins and the future of microfluidics, Nature 442 (7101) (2006) 368–373. doi:10.1038/nature05058.

[2] E. K. Sackmann, A. L. Fulton, D. J. Beebe, The present and future role of microfluidics in biomedical research, Nature 507 (7491) (2014) 181–189. doi:10.1038/nature13118.

[3] X. Xuan, J. Zhu, C. Church, Particle focusing in microfluidic devices, Microfluid. Nanofluidics 9 (1) (2010) 1–16. doi:10.1007/s10404-010-0602-7.

[4] G. D'Avino, P. L. Maffettone, Particle dynamics in viscoelastic liquids, J. Non-Newtonian Fluid Mech. 215 (2015) 80–104. doi:10.1016/j.jnnfm.2014.09.014.

[5] S. Yang, J. Y. Kim, S. J. Lee, S. S. Lee, J. M. Kim, Sheathless elasto-inertial particle focusing and continuous separation in a straight rectangular microchannel, Lab Chip 11 (2) (2011) 266–273. doi:10.1039/c0lc00102c.

[6] G. D'Avino, G. Romeo, M. M. Villone, F. Greco, P. A. Netti, P. L. Maffettone, Single line particle focusing induced by viscoelasticity of the suspending liquid: theory, experiments and simulations to design a micropipe flow-focuser, Lab Chip 12 (9) (2012) 1638–1645. doi:10.1039/c2lc21154h.

[7] K. W. Seo, H. J. Byeon, H. K. Huh, S. J. Lee, Particle migration and

single-line particle focusing in microscale pipe flow of viscoelastic fluids, RSC Adv. 4 (7) (2014) 3512–3520. doi:10.1039/c3ra43522a.

[8] G. D'Avino, P. L. Maffettone, F. Greco, M. A. Hulsen, Viscoelasticity-induced migration of a rigid sphere in confined shear flow, J. Non-Newtonian Fluid Mech. 165 (9-10) (2010) 466–474. doi:10.1016/j.jnnfm.2010.01.024.

[9] D. C. Tretheway, C. D. Meinhart, Apparent fluid slip at hydrophobic microchannel walls, Phys. Fluids 14 (3) (2002) L9–L12. doi:10.1063/1.1432696.

[10] E. Lauga, M. P. Brenner, H. A. Stone, Microfluidics: the no-slip boundary condition. In: C. Tropea, A. L. Yarin, J. F. Foss (Eds.), Springer handbook of experimental fluid mechanics, Springer, New York, 2007, Ch. 19, pp. 1219–1240.

[11] M. A. Tehrani, An experimental study of particle migration in pipe flow of viscoelastic fluids, J. Rheol. 40 (6) (1996) 1057–1077. doi:10.1122/1.550773.

[12] S. G. Hatzikiriakos, Slip mechanisms in complex fluid flows, Soft Matter 11 (40) (2015) 7851–7856. doi:10.1039/c5sm01711d.

[13] C. L. M. H. Navier, Mémoire sur les lois du mouvement des fluides, Mémoires de l'Académie Royale des Sciences de l'Institut de France 6 (1823) 389–440.

[14] E. Lauga, T. M. Squires, Brownian motion near a partial-slip boundary:

A local probe of the no-slip condition, Phys. Fluids 17 (10) (2005) 103102. doi:10.1063/1.2083748.

[15] H. Luo, C. Pozrikidis, Effect of surface slip on Stokes flow past a spherical particle in infinite fluid and near a plane wall, J. Eng. Math. 62 (1) (2008) 1–21. doi:10.1007/s10665-007-9170-6.

[16] H. J. Keh, Y. C. Chang, Creeping motion of a slip spherical particle in a circular cylindrical pore, Int. J. Multiphase Flow 33 (7) (2007) 726–741. doi:10.1016/j.ijmultiphaseflow.2006.12.008.

[17] M. Trofa, G. D'Avino, M. A. Hulsen, F. Greco, P. L. Maffettone, Numerical simulations of the dynamics of a slippery particle in newtonian and viscoelastic fluids subjected to shear and poiseuille flows, J. Non-Newtonian Fluid Mech. 228 (2016) 46–54. doi:10.1016/j.jnnfm.2015.12.001.

[18] R. G. Larson, Constitutive equations for polymer melts and solutions, Butterworth, Boston, 1988.

[19] A. C. B. Bogaerds, M. A. Hulsen, G. W. M. Peters, F. P. T. Baaijens, Stability analysis of injection molding flows, J. Rheol. 48 (4) (2004) 765–785. doi:10.1122/1.1753276.

[20] H. H. Hu, N. A. Patankar, M. Y. Zhu, Direct numerical simulations of fluid-solid systems using the arbitrary Lagrangian-Eulerian technique, J. Comput. Phys. 169 (2) (2001) 427–462. doi:10.1006/jcph.2000.6592.

[21] G. D'Avino, M. A. Hulsen, Decoupled second-order transient schemes for the flow of viscoelastic fluids without a viscous solvent contribution, J.

Non-Newtonian Fluid Mech. 165 (23) (2010) 1602–1612. doi:10.1016/j.jnnfm.2010.08.007.

[22] A. C. B. Bogaerds, M. A. Hulsen, G. W. M. Peters, F. P. T. Baaijens, Time dependent finite element analysis of the linear stability of viscoelastic flows with interfaces, J. Non-Newtonian Fluid Mech. 116 (1) (2003) 33–54. doi:10.1016/s0377-0257(03)00099-5.

[23] A. N. Brooks, T. J. R. Hughes, Streamline upwind/Petrov-Galerkin formulations for convection dominated flows with particular emphasis on the incompressible Navier-Stokes equations, Comput. Methods Appl. Mech. Eng. 32 (1-3) (1982) 199–259. doi:10.1016/0045-7825(82)90071-8.

[24] R. Fattal, R. Kupferman, Constitutive laws for the matrix-logarithm of the conformation tensor, J. Non-Newtonian Fluid Mech. 123 (2-3) (2004) 281–285. doi:10.1016/j.jnnfm.2004.08.008.

[25] M. A. Hulsen, R. Fattal, R. Kupferman, Flow of viscoelastic fluids past a cylinder at high Weissenberg number: Stabilized simulations using matrix logarithms, J. Non-Newtonian Fluid Mech. 127 (1) (2005) 27–39. doi:10.1016/j.jnnfm.2005.01.002.

[26] B. P. Ho, L. G. Leal, Inertial migration of rigid spheres in two-dimensional unidirectional flows, J. Fluid Mech. 65 (1974) 365–400. doi:10.1017/S0022112074001431.

[27] J. Bikard, P. Menard, E. Peuvrel-Disdier, T. Budtova, 3d numerical simulation of the behaviour of a spherical particle suspended in a newtonian

fluid and submitted to a simple shear, Comput. Mater. Sci. 37 (4) (2006) 517–525. doi:10.1016/j.commatsci.2005.12.003.